

# Supporting Information for

## Topological band engineering of Lieb lattice in phthalocyanine-based metal-organic frameworks

Wei Jiang,<sup>†</sup> Shunhong Zhang,<sup>‡</sup> Zhengfei Wang,<sup>¶</sup> Feng Liu,<sup>§,\*</sup> and Tony Low<sup>†,\*</sup>

<sup>†</sup>Department of Electrical and Computer Engineering, University of Minnesota,  
Minneapolis, MN 55455, USA

<sup>‡</sup>International Center for Quantum Design of Functional Materials, Hefei National Laboratory for Physical Sciences at Microscale, and CAS Center For Excellence in Quantum Information and Quantum Physics, University of Science and Technology of China, Hefei, Anhui 230026, China

<sup>¶</sup>Hefei National Laboratory for Physical Sciences at the Microscale, University of Science and Technology of China, Hefei, Anhui, 230026, China

<sup>§</sup>Department of Materials Science and Engineering, University of Utah,  
Salt Lake City, UT 84102, USA

\*Corresponding author; E-mail: fliu@utah.edu; tlow@umn.edu.

### **This PDF file includes:**

- 1: DFT calculation methods
- 2: Tight-binding analysis
- 3: Topological characterization
- 4: Time-reversal symmetry broken QSH effect
- 5: LDA and LDA+U calculations of magnetic CuPc-MOF

Supporting figures: 1 to 7

## DFT calculation methods

The properties of MPC-based MOFs were calculated using first-principles methods based on density functional theory (DFT), as embedded in the Vienna ab initio simulation package code. The projected augmented wave method with the generalized gradient approximation (GGA) exchange-correlation potential was applied. All self-consistent calculations were performed with a plane wave cutoff energy of 500 eV. Geometric optimizations were carried out without any constraint until the force on each atom is less than  $0.01 \text{ eV}\cdot\text{\AA}^{-1}$  and the change of total energy per cell is smaller than  $10^{-4} \text{ eV}$ . For monolayer MPC-MOF crystalline calculations, the Brillouin zone K-mesh sampling was set as  $15\times 15\times 1$ . To eliminate the interaction between layers along the  $z$  direction, we introduced a vacuum layer with thickness of  $15 \text{ \AA}$ . The lattice constant  $a$  was fully relaxed. To better describe the localized  $3d$  electrons of transition metals, additional on-site Hubbard  $U$  terms were added in calculations. Different  $U$  values were tested.

## Tight-binding analysis

To understand the intriguing physical properties of Lieb-lattice system [Fig. S1(a)], we start from the fundamental Hamiltonian of Lieb-lattice with only the nearest-neighbor (NN,  $t$ ) and the next-NN (NNN,  $t'$ ) hoppings:

$$\mathcal{H}_0 = \sum_i \epsilon_i c_i^\dagger c_i + \sum_{\langle i,j \rangle} t c_i^\dagger c_j + \sum_{\langle\langle i,j \rangle\rangle} t' c_i^\dagger c_j + H.c., \quad (1)$$

where  $\epsilon_i$  is the on-site energy (OSE) on site  $i$ , which is set to be the same for edge-center sites, A and C. The energy difference between B and A sites is defined as  $\Delta E = \epsilon_B - \epsilon_A$ . The well-known Lieb lattice is studied in the ideal case with both  $t'$  and  $\Delta E$  equal to zero. By transforming  $\mathcal{H}_0$  into momentum space using  $\mathcal{H} = \sum_k \Psi_k^\dagger H(k) \Psi_k$ , where  $\Psi_k^\dagger = (c_{Ak}^\dagger, c_{Bk}^\dagger, c_{Ck}^\dagger)$ .

We get the matrix Hamiltonian for the ideal scenario:

$$H(k) = \begin{pmatrix} 0 & -2t \cos(\vec{k} \cdot \frac{\vec{v}_1}{2}) & -2t \cos(\vec{k} \cdot \frac{\vec{v}_2}{2}) \\ -2t \cos(\vec{k} \cdot \frac{\vec{v}_1}{2}) & 0 & 0 \\ -2t \cos(\vec{k} \cdot \frac{\vec{v}_2}{2}) & 0 & 0 \end{pmatrix}.$$

The analytical solutions are  $E_1 = 0$  and  $E_{2,3} = \pm 2t \sqrt{\cos^2(\vec{k} \cdot \frac{\vec{v}_1}{2}) + \cos^2(\vec{k} \cdot \frac{\vec{v}_2}{2})}$ , which leads to the ideal flat band in the middle of Dirac bands, as shown in Fig. S1(b). Different from trivial flat band due to localized states without interaction, the flat band here is due to structural destructive interference with a finite hopping  $t$ , which is proposed to hold, for example, intriguing superconductivity, ground state ferromagnetism, and fractional quantum Hall state. With a non-zero  $\Delta E$ , the matrix Hamiltonian changes to

$$H(k) = \begin{pmatrix} \Delta E & -2t \cos(\vec{k} \cdot \frac{\vec{v}_1}{2}) & -2t \cos(\vec{k} \cdot \frac{\vec{v}_2}{2}) \\ -2t \cos(\vec{k} \cdot \frac{\vec{v}_1}{2}) & 0 & 0 \\ -2t \cos(\vec{k} \cdot \frac{\vec{v}_2}{2}) & 0 & 0 \end{pmatrix}.$$

The resulted eigenstates are  $E_{2,3} = \left\{ \Delta E \pm \sqrt{(\Delta E)^2 + 16t^2 [\cos^2(\vec{k} \cdot \frac{\vec{v}_1}{2}) + \cos^2(\vec{k} \cdot \frac{\vec{v}_2}{2})]} \right\} / 2$  and  $E_1 = 0$ . The dispersion of upper and lower Dirac bands remain symmetric with a quenched bandwidth because of the decrease of the effective “ $t$ ”. The middle flat band remains the same as the ideal case, while the triple degeneracy at  $M$  point is lifted by moving upper/lower Dirac band away from the flat band for positive/negative  $\Delta E$ , as shown in Fig. S1(c) and (d). The corresponding band gap equals to  $\Delta E$ , which is the OSE difference between the corner and edge-center states. It is important to mention that due to nonzero  $\Delta E$ , the topological invariant for the three bands changes accordingly, while there is still a double degeneracy between the Dirac and flat band at the  $M$  point, making the system remains topological nontrivial.

When further considering the NNN hopping effect with nonzero  $t'$ , the corresponding matrix Hamiltonian evolves to:

$$H(k) = \begin{pmatrix} \Delta E & -2t \cos(\vec{k} \cdot \frac{\vec{v}_1}{2}) & -2t \cos(\vec{k} \cdot \frac{\vec{v}_2}{2}) \\ -2t \cos(\vec{k} \cdot \frac{\vec{v}_1}{2}) & 0 & -4t' \cos(\vec{k} \cdot \frac{\vec{v}_1}{2}) \cos(\vec{k} \cdot \frac{\vec{v}_2}{2}) \\ -2t \cos(\vec{k} \cdot \frac{\vec{v}_2}{2}) & -4t' \cos(\vec{k} \cdot \frac{\vec{v}_1}{2}) \cos(\vec{k} \cdot \frac{\vec{v}_2}{2}) & 0 \end{pmatrix},$$

where the NNN hopping term  $H_{AC}$  is added as  $-4t' \cdot \cos(\vec{k} \cdot \frac{\vec{v}_1}{2}) \cdot \cos(\vec{k} \cdot \frac{\vec{v}_2}{2})$ . Clearly, when  $k_x$  or  $k_y$  equals zero,  $H_{AC}$  term becomes zero. Therefore, the band structure along  $M - X/Y$  remains the same as the case without  $H_{AC}$ , so does the corresponding topological properties related to the  $M$  point degeneracy. The band structure along other k-paths do change with the inclusion of  $H_{AC}$ , where the middle band becomes no longer flat across the whole Brillouin zone and tends to getting close to one of the Dirac band. Specially, when  $t' = \pm 0.5t$ , it contact with the lower/upper Dirac band at the  $\Gamma$  point. With further increasing of the  $t'$ , the middle band and Dirac band cross at some points between  $\Gamma$  and  $M$ , leading to the formation of type-II Dirac point.

## Topological characterization

Topological properties are studied by adding one NNN spin-orbit coupling (SOC) term,  $H_{SOC}$ :

$$\mathcal{H}_{soc} = i\lambda \sum_{\langle\langle i,j \rangle\rangle} v_{ij} c_i^\dagger \sigma_z c_j + H.C., \quad (2)$$

where  $\lambda$  describes the SOC strength,  $\sigma_z$  is the Pauli matrix,  $v_{ij}$  corresponds to the magnetic flux, which can be viewed as a hopping phase with positive/negative unit for clockwise/anti-clockwise case. The nontrivial topology of the systems can be further confirmed through the topological invariant calculation, *i.e.*, Chern number ( $C$ ), based on Kubo formula using :

$$C = \frac{1}{2\pi} \int_{BZ} d^2 \vec{k} \Omega(\vec{k}), \quad \Omega(\vec{k}) = \sum_n f_n \Omega_n(\vec{k}), \quad (3)$$

$$\Omega_n(\vec{k}) = - \sum_{n' \neq n} 2Im \frac{\langle \Psi_{nk} | \hat{v}_x | \Psi_{n'k} \rangle \langle \Psi_{n'k} | \hat{v}_y | \Psi_{nk} \rangle}{(\epsilon_{n'k} - \epsilon_{nk})^2}, \quad (4)$$

where  $n$  is the band index here,  $\Psi_{nk}$  and  $\epsilon_{nk}$  are the eigenstate and eigenvalue of the band  $n$ , respectively.  $f_n$  is the Fermi distribution function,  $\hat{v}_{x/y}$  is the velocity operator. The Chern numbers of different bands for different systems are calculated, where the bottom and the top

bands have a nonzero Chern number ( $\pm 1$ ) and the middle band has a zero Chern number for the ideal scenario. After adding the OSE difference term  $\Delta E$ , the Chern number for the isolated Dirac band changes to zero, while the remaining two bands that in contact having a nonzero Chern number ( $\pm 1$ ). Further inclusion of the NNN hopping interaction does not change the topological invariant before the isolated band contacts the middle band. This is consistent with our previous conclusions that the topological properties are mainly related to the  $M$  point features. After the band closing with  $t' > -0.5t$ , the topological invariant becomes the same as the ideal one again. Similarly, calculations of the evolution of Wannier charge centers and the Berry curvature distribution can further confirm the topological features, as shown in Fig. S6 for the  $t' = -0.5t$  and  $\Delta E > 0$  scenario.

As a cross check, we also characterize the topological nature of the strained ZnPc by calculating its  $Z_2$  number. Considering the system has spatial inversion symmetry, its  $Z_2$  invariant can be computed according to the Fu-Kane formalism, which simply counts the number of odd parity occupied states at the time-reversal invariant points. Based on our calculations, the numbers of occupied states with odd parity are 37, 42, 42, and 38 at  $\Gamma$ , X, Y, and M points, leading to a  $Z_2$  invariant of 1, again confirming that the 2D sheet is topologically nontrivial under strain.

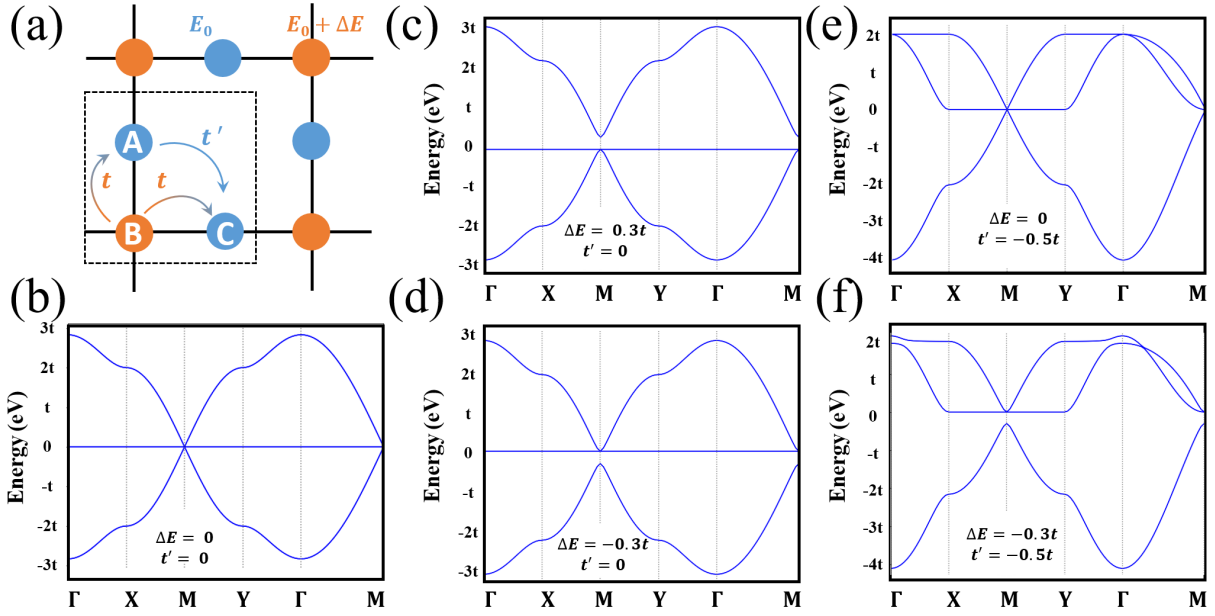
## **Time-reversal symmetry broken QSH effect**

It is important to mention that to observe the time-reversal symmetry broken QSH effect, systems are required to have both weak electron-electron interaction and disorder. Because the Lieb-electrons in MPC-MOF system are mainly contributed by the p-orbitals of the organic ligands, their electron-electron interaction should be quite small. Meanwhile, due to the delocalization nature of the  $\pi$ -conjugation bands near the Fermi level, the on-site coulomb interaction could be very small too. Therefore, it is reasonable to expect the time-reversal symmetry broken QSH effect to be observed in MPC-MOF system. On the other hand, the SOC gap and the

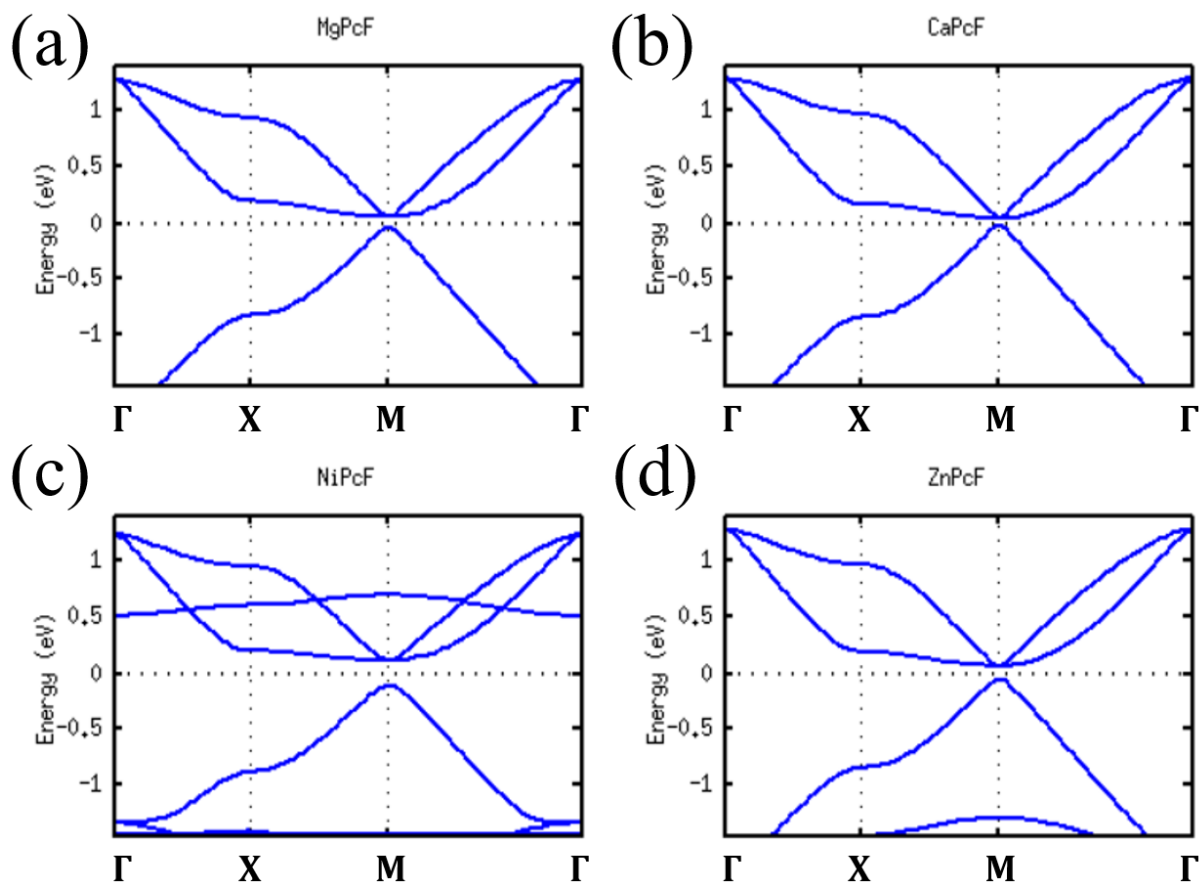
stability of the MPc-MOF are also very important, which require a large SOC gap and stable structure with weak disorder. These could possibly be achieved by selecting metal elements with large intrinsic SOC and choosing high-quality substrates.

## **LDA and LDA+U calculation for magnetic MPc-MOF**

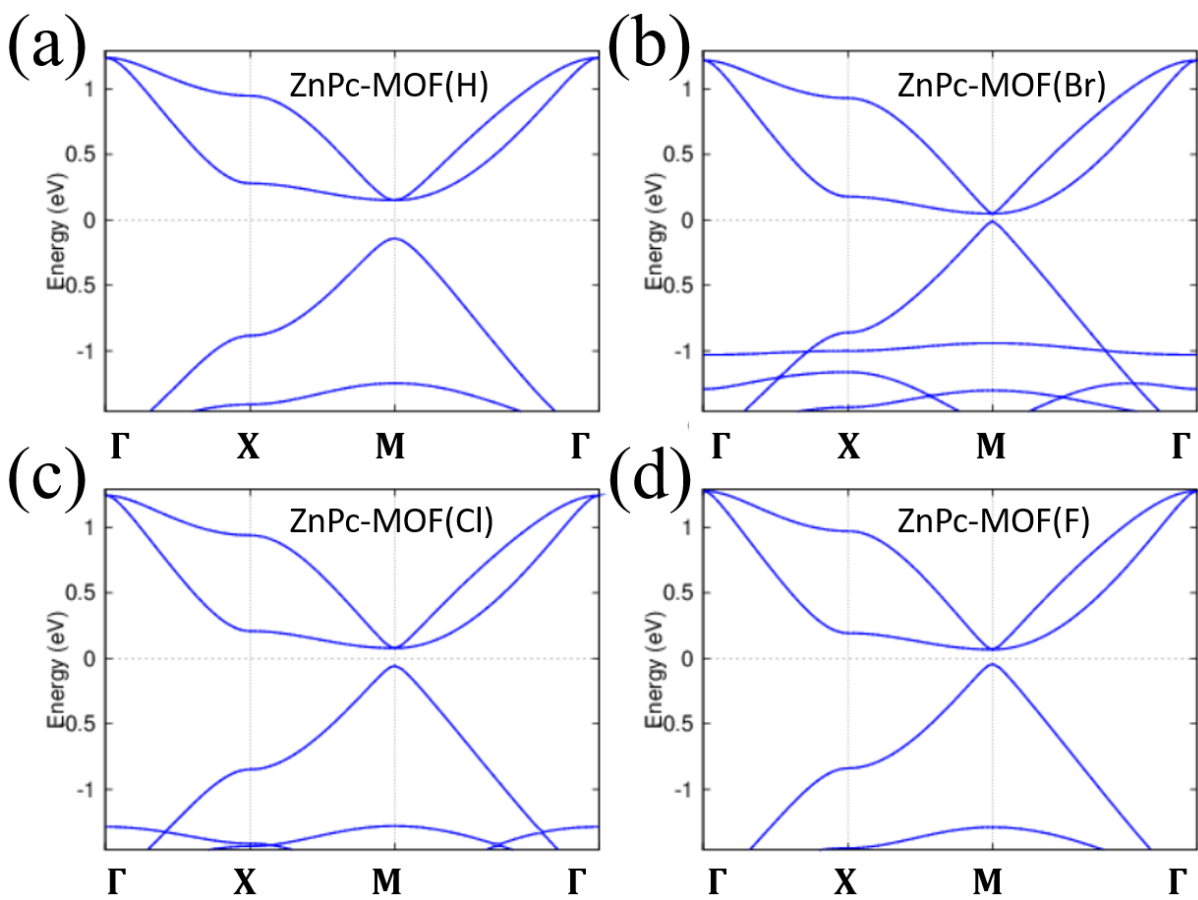
To understand the electronic and magnetic properties of magnetic MPc-MOF, we used CuPc-MOF as a representative example for detailed studies. We first performed DFT LDA calculation by purposely turning of the spin degree of freedom, which usually can provide very fundamental information about the electronic properties of the system. The band structure shows one isolated band right at the Fermi level besides the three Lieb bands as observed in nonmagnetic systems [Fig. S7(a)]. The band at the Fermi level is mainly contributed by Cu  $d$  electrons that is exactly half-filled, consistent with  $d^9$  electronic configuration of  $\text{Cu}^{2+}$ . The missing of localized spin state is the known failure of the LDA when treating the strong correlation effect. A common remedy is to apply the LDA+U calculation to properly treat the localized  $d$  electrons. Our LDA+U ( $U=4$  eV,  $J=0.9$  eV) calculation shows clearly isolated spin-up and spin-down bands separated by the Fermi level, consistent with the physical picture of localized  $S=1/2$  spins [Fig. S7(b)]. We further tested different  $U$  values, which solely modifies the gap size between the spin-up and spin-down band and does not change the physics [Fig. S7(b)-(f)]. The intrinsic system is therefore a magnetic insulator. Because of the direct band gap at the  $M$  point is due to the charge transfer induced by the OSE difference between corner and edge-center state, the system is intrinsically, therefore, topological trivial. Interestingly, we notice the Lieb-bands are also spin splitted and shift the same direction as the Cu local spins, indicating a ferromagnetic interaction between the itinerant  $\pi$  electrons with the localized Cu spins.



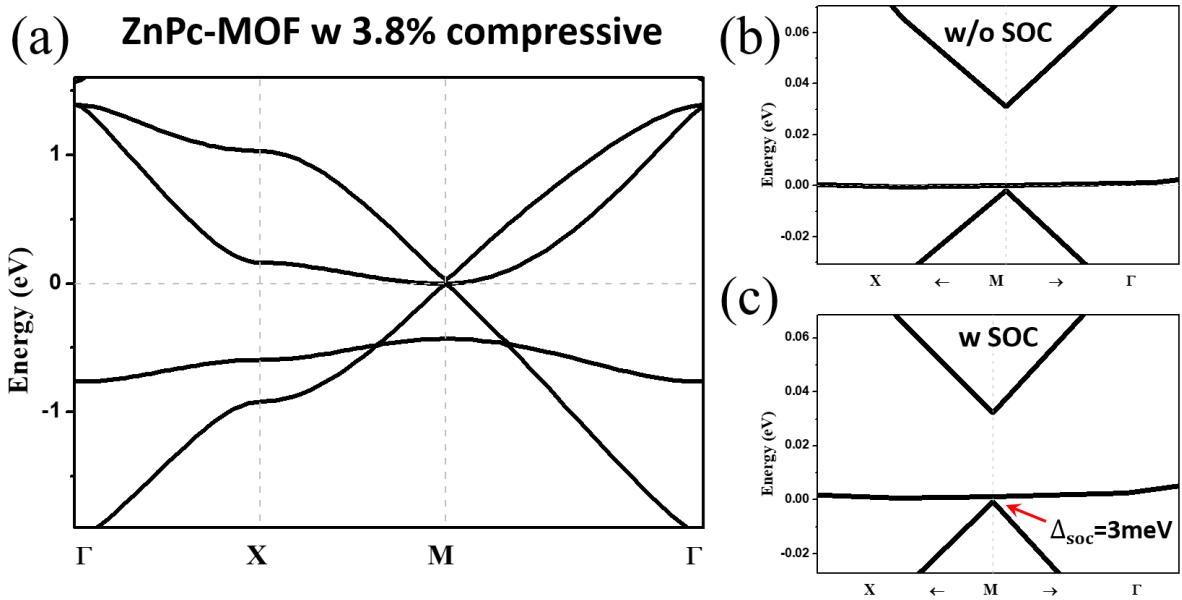
**Supplementary Figure S1. Tight-binding analysis of the 2D Lieb-lattice model.** (a) Lieb-lattice structure with one corner and two edge-center states. (b) Band structure of ideal Lieb lattice. (c) and (d) Non-ideal Lieb lattice with positive and negative OSE  $\Delta E$  that open a charge transfer gap above and below the middle flat band, respectively. (e) and (f) Strongly distorted Band structure of Lieb lattice due to the NNN interaction ( $t' = 0.5t$ ) for the case without and with negative  $\Delta E$ , respectively.



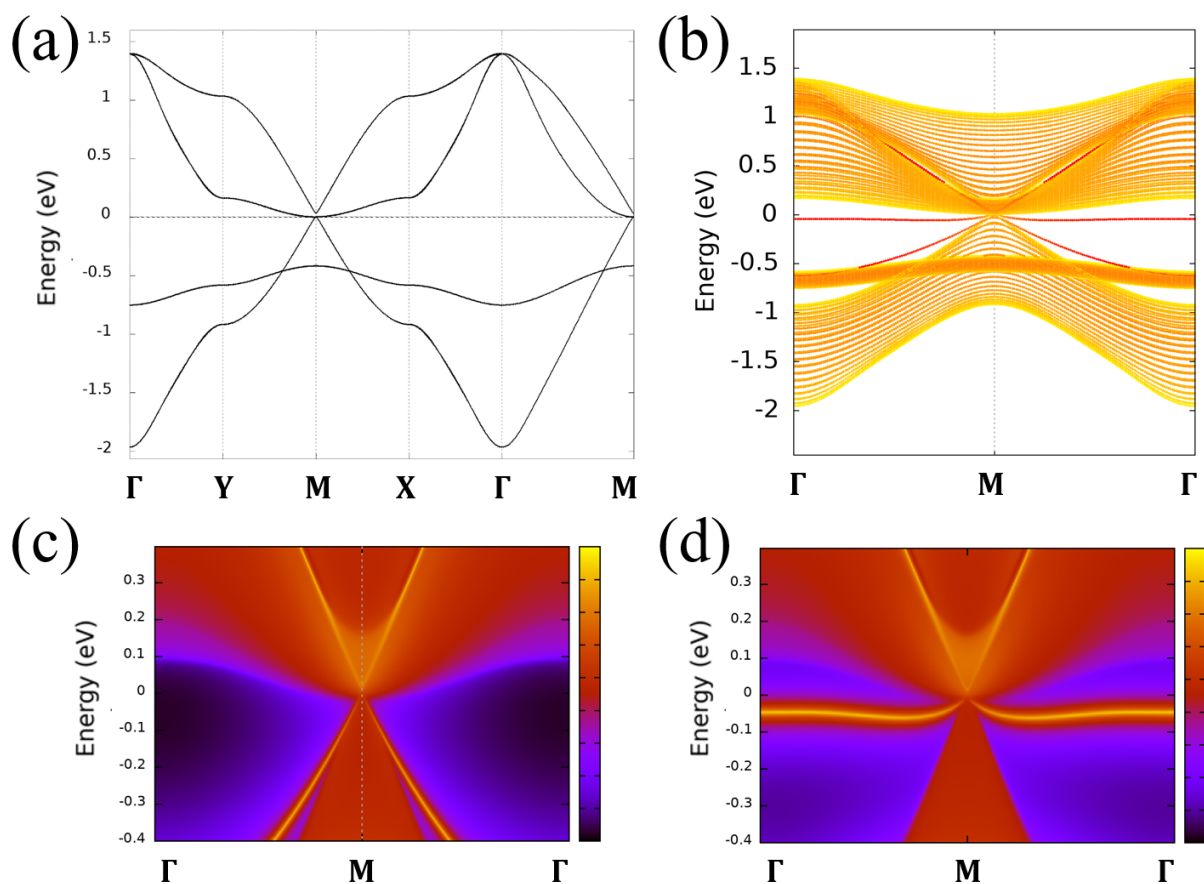
**Supplementary Figure S2. Band structure engineering by modifying local chemical potential of corner state.** (a) Band structure of MgPc-MOF. (b)-(d) Same as (a) for CaPc-MOF, NiPc-MOF, and ZnPc-MOF, respectively.



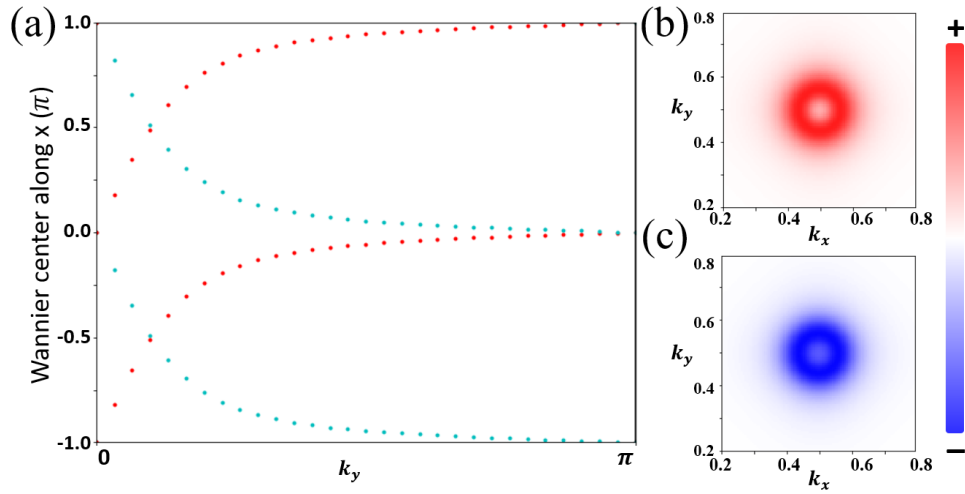
**Supplementary Figure S3. Band structure engineering by changing local chemical potential of edge-center state.** (a) Band structure of ZnPc-MOF with H. (b)-(d) Same as (a) for ZnPc-MOF with Br, Cl, and F replacing H, respectively.



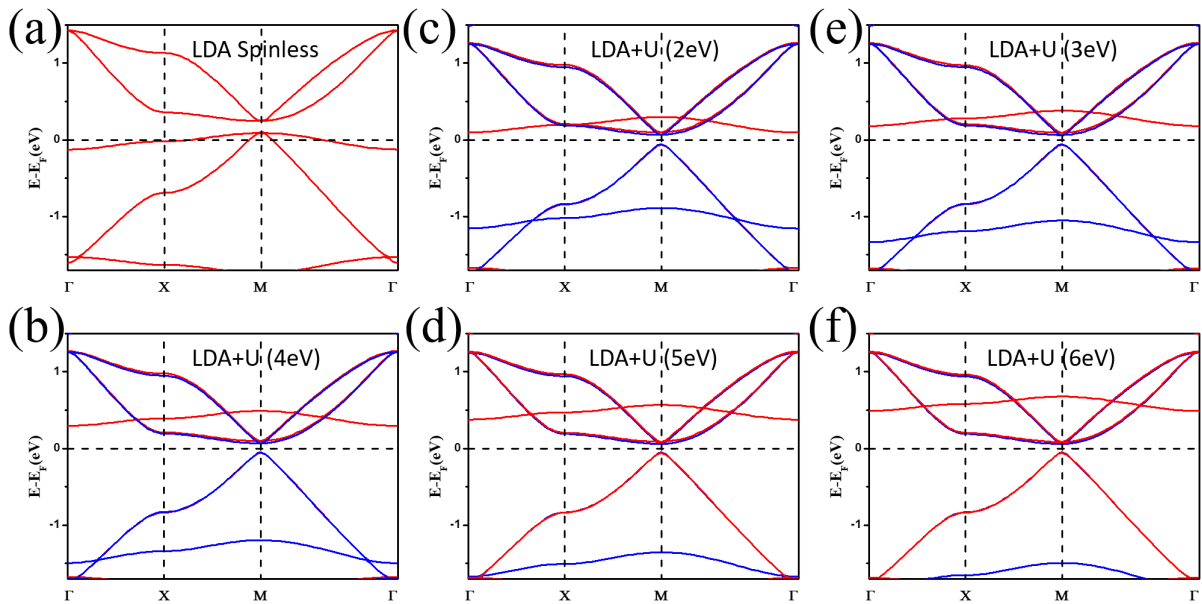
**Supplementary Figure S4. Spin-orbit coupling effect to the band structure.** (a) Band structure of ZnPc-MOF with a compressive strain of 3.8% without SOC, showing the gap closing between the middle and lower Dirac bands. (b) and (c) Enlarged band structure near Fermi level around  $M$  point without and with SOC, respectively. A gap of around 3 meV at  $M$  point induced by SOC indicates the topological nontrivial states.



**Supplementary Figure S5. Topological edge states of strained ZnPc-MOF.** (a) Maximally localized Wannier function fitted band structure using Wannier90 package. (b) Band structure of ribbon calculation of ZnPc-MOF, which shows clear edge states (red color) that connect bulk state (yellow color). (c) and (d) Surface states calculation based on Wannier fitted TB Hamiltonian with a semi-infinite structure using Green's function, where yellow highlighted states indicate the topological surface state.



**Supplementary Figure S6. Evolution of Wannier charge center and the Berry curvature of strained ZnPc-MOF.** (a) The evolution of Wannier charge center for the bottom spin-up/down (blue/red colored dots) Dirac bands, yielding an accumulation of  $\pm\pi$  that confirms the topological insulator state. (b) Spin Berry curvature for spin-up/down states with red and blue color representing positive and negative values.



**Supplementary Figure S7. LDA spinless and LDA+U spin polarized calculation of CuPc-MOF.** (a) Band structure of CuPc-MOF based on LDA spinless calculation. (b)-(f) Same as (a) for LDA+U calculations with different U values.